

# Optical and gas sensing properties of SnO<sub>2</sub> nanowires grown by vapor–liquid–solid mechanism

Muhammad Amin<sup>1</sup> · Muhammad Saeed Akhtar<sup>2</sup> · Khuram Shahzad Ahmad<sup>3</sup> ·  
Yousef Alghamdi<sup>4</sup> · Neerish Revaprasadu<sup>5</sup> · Mohammad Azad Malik<sup>5,6</sup> ·  
Nazar Abbas Shah<sup>7</sup>

Received: 28 April 2017 / Accepted: 17 August 2017 / Published online: 13 September 2017  
© Springer Science+Business Media, LLC 2017

**Abstract** SnO<sub>2</sub> nanowires were synthesized via vapor transport method by modulating the thickness of the Gold (Au) catalyst. The effect of morphology and photoluminescence properties of nanowires on gas sensing was investigated. The structural and morphological studies reveal that the synthesized nanowires are crystalline in nature with high density. The nanowires were evenly spread on the surface of the substrate. These nanowires were tested for gas sensing properties based on change in resistance under exposure to air and gases (CO, CH<sub>4</sub>, Methanol). The results showed an improved response as compared to the previous studied. These sensors have potential applications in advanced sensing devices.

## 1 Introduction

One-dimensional (1D) nanostructures have attracted great interests due to their outstanding properties and potential applications in last two decades [1–3]. There has been an increasing demand for highly sensitive and selective gas-sensing devices in many fields such as environmental monitoring, security systems and health care systems [4, 5]. Tin Oxide (SnO<sub>2</sub>) is one of the most important sensing material and widely used as a metal oxide semiconductor gas sensor [6], mainly due to its sensitivity towards different gases [7]. Sensitivity of sensors depends upon the thickness of the depletion layer when the dimension of sensor material is comparable to the thickness of that layer [8]. Therefore different nanostructures such as nano-powders [9], nanowires [10–13], nanotubes [14–16] and nano-belts [17–19] are being used for UV light and gas sensing owing to their high surface to volume ratios. Recently, authors have reported the CO gas sensing mechanism of both un-doped and Mg doped ZnO nanostructures [20]. Yamazoe et al. proposed that by reducing the crystallite size of nanomaterials, sensitivity and energy consumption of metal oxide gas sensors can be achieved [21]. Nanowires with Debye length (thickness of the space charge layer) having small diameter and high surface-to-volume ratio are of much importance. It is already established that sensitivity and response time of sensors significantly depend on the processes taking place at the surfaces of nanostructures [22, 23]. Sensing models on space charge region for various nanostructures have been presented by Yamazoe et al. and Hernandez-Ramirez et al. [24, 25]. Zhang et al. reported that the sensitivity of single crystalline 1D SnO<sub>2</sub> nanocrystals with controllable sizes had closely related to the specific surface area of these nanocrystals [26]. Lipeng et al. proposed square-shaped and single crystalline SnO<sub>2</sub> nanowires synthesized by hydrothermal

✉ Nazar Abbas Shah  
nabbasqureshi@yahoo.com; nazar\_abbas@comsats.edu.pk

Muhammad Saeed Akhtar  
saeed\_khakhi@yahoo.com

- <sup>1</sup> Centres of Excellence in Science & Applied Technologies, H-11/4, Islamabad, Pakistan
- <sup>2</sup> Division of Science and Technology, University of Education, College Road, Township, Lahore, Pakistan
- <sup>3</sup> Environmental Sciences Department, Fatima Jinnah Women University, The Mall, Rawalpindi, Pakistan
- <sup>4</sup> Department of Chemistry, Faculty of Science and Art-Rabigh, King Abdulaziz University, Jeddah, Saudi Arabia
- <sup>5</sup> Department of Chemistry, University of Zululand, Private Bag X1001, Kwa-Dlangezwa 3880, South Africa
- <sup>6</sup> Schools of Materials, The University of Manchester, Oxford Road, Manchester M13 9PL, UK
- <sup>7</sup> Thin Films Technology Laboratory, Department of Physics, COMSATS Institute of Information Technology (CIIT), Islamabad 45550, Pakistan

method and observed that these nanostructures exhibit good sensitivity, excellent stability and selectivity in addition to quick response and short recovery times under exposure to acetone gas [27]. Kalmakov et al. proposed the improvement in sensitivity of Pd functionalized SnO<sub>2</sub> nanowires towards oxygen and hydrogen and observed that gas sensitivity of these nanostructures depends on the catalytic dissociation on Pd nanoparticle surfaces and the subsequent diffusion of atomic species onto the surface of oxide [28]. Kwon et al. recently reported the NO<sub>2</sub> gas sensing behavior of SnO<sub>2</sub> nanowires and observed that Sn interstitials are responsible for improvement in enhanced sensing response [29]. Jin Wu et al. also fabricated SnO<sub>2</sub> zigzag nanobelts via catalyst assisted carbothermal reaction of SnO<sub>2</sub> powder [30]. Dang et al. presented the chlorine gas sensing of ZnO, WO<sub>3</sub> and SnO<sub>2</sub> nanowire sensors at low temperatures [31]. Most recently, Zheng et al. proposed the modeling and simulation of individual SnO<sub>2</sub> nano-belt gas sensors with FET structure and observed the output characteristics of the device by employing a modified drift–diffusion model and taking into account the quantum mechanical effects [32]. Various approaches have been used to fabricate SnO<sub>2</sub> nanomaterials, such as the molten salt method [33], carbothermal reduction method [34], laser ablation vapor deposition [24, 25], hydrothermal method [26], and plasma treatment [16]. Among them, vapor transport growth is one of the most widely used methods due to its low cost and flexibility [35]. Different source precursors such as SnO [36–41], SnO<sub>2</sub> [35], SnO/graphite [42–45] and SnO<sub>2</sub>/graphite have been used in previous studies [46].

In the present work, the effective control of the diameter and effect of surface defects on SnO<sub>2</sub> nanowires for gas sensors by a simple vapor liquid solid (VLS) mechanism have been demonstrated. SnO<sub>2</sub> nanowire-network-based gas sensor for CO gas sensing properties as a function of diameter (aspect ratio) and surface defects is evaluated. These results show improved sensing response compared to that reported earlier in terms of sensitivity and limit of detection.

## 2 Experimental

### 2.1 Chemicals

The reagents, SnO<sub>2</sub> (99.99%) and graphite (99.99%) powders were purchased from Sigma-Aldrich and used without further purification. Au was used as catalyst. Isopropyl alcohol (IPA) and acetone were used for cleaning of substrates.

### 2.2 Instruments

Ion sputtering of Au layer was deposited on Si substrates by JFC 1500 sputtering unit. Ball milling was performed in

zirconia jar and zirconia balls were used for this purpose. The crystallinity, morphology and elemental composition were determined by using powder X-ray diffraction (p-XRD, X'Pert PRO Diffractometer, PANalytical with Cu K $\alpha$  radiation  $\lambda = 1.5418 \text{ \AA}$ ), scanning electron microscopy (SEM, Hitachi SU 1500), transmission electron microscopy (TEM) and energy dispersive X-ray spectroscopy (EDX). Optical properties of the synthesized nanostructures were carried out by absorption spectroscopy (lambda 950 UV–Vis spectrophotometer) and photoluminescence (PL, DONGWOO Optron, 325 nm Ar laser). Gas sensing experiments were performed via two probe method at room temperature using a Keithly 2100 multimeter.

### 2.3 Synthesis of SnO<sub>2</sub> nanowires and fabrication of gas sensors

SnO<sub>2</sub> nanowires were synthesized by vapor transport method on n-type Si (100) substrates using VLS mechanism as shown in Fig. 1a. Substrates were ultrasonically cleaned in IPA and acetone prior to deposition. Au catalyst layer was deposited by ion sputtering technique. The thickness of catalyst layer was controlled in-situ during ion sputtering by film thickness monitor. Three Si substrates were prepared having Au catalyst layers of 1, 2 and 5 nm thickness. For deposition of SnO<sub>2</sub> nanowires, SnO<sub>2</sub> and graphite powders with weight ratio of 4:1 were mixed in a ball mill for 2 h and then loaded in a ceramic boat. Ball milling was performed in zirconia jar and zirconia balls were used for this purpose instead of stainless steel balls as reported by Butt et al. [47]. Ceramic boat containing the mixture was placed at the center of a quartz tube with dimensions as 3.5 cm in diameter and 100 cm in length which then transferred to furnace. Three experiments were performed on Si substrates having 1, 2 and 5 nm of Au catalyst layers while all the experimental parameters were kept same. The synthesis temperature of the VLS process was maintained at 900 °C for 45 min in the nitrogen atmosphere with a constant flow rate of 60 sccm. The furnace was cooled down to room temperature after completion of experiment and substrates were collected for various characterizations.

The gas sensors were fabricated by using the technique reported earlier by authors [20] and gas sensing experiments were performed via two probe method at room temperature using a Keithly 2100 multimeter. The sensing response ( $S = R_a/R_g$ ) of the device was measured by the resistance change upon exposure to air ( $R_a$ ) and test gas ( $R_g$ ) in a home-built gas chamber connected to a multimeter, gas flow meters and tube furnace. The schematic design of sensor and gas sensing setup are shown in Fig. 1b–d. A photograph of gas sensing setup with an inset showing sensor and pressure contacts (Fig. 1d).

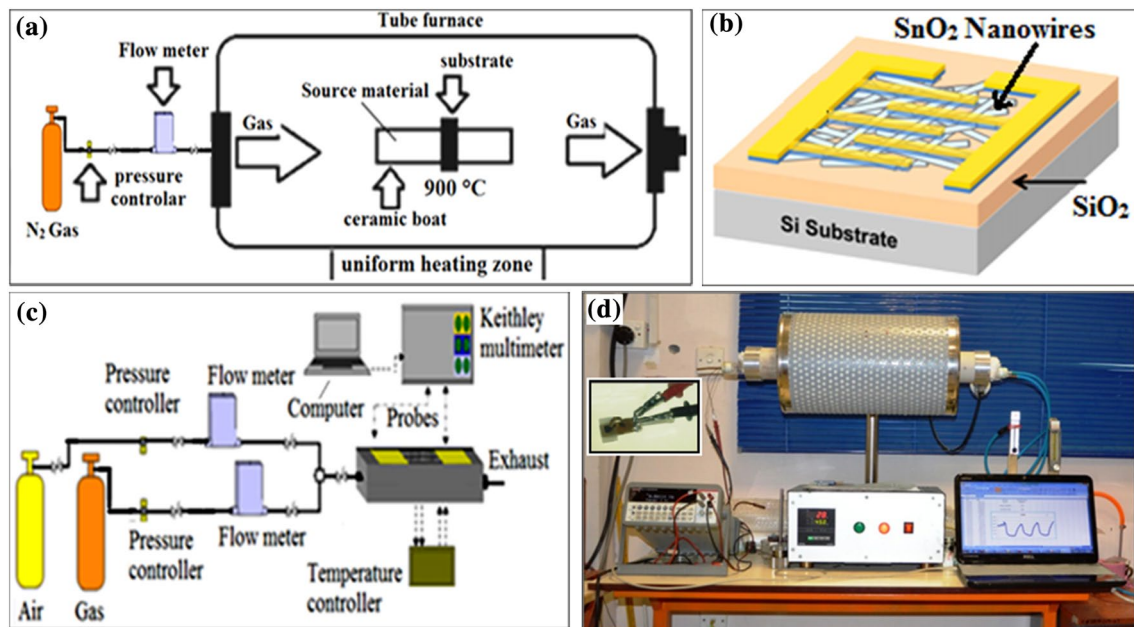


**Fig. 1** **a** Experimental setup of furnace for synthesis of nanowires. **b** Schematic of fabricated SnO<sub>2</sub> Nanowires sensor. **c** Gas sensing setup. **d** Photograph of gas sensing experimental setup and sensor with pressure contacts (*inset*)

### 3 Results and discussion

#### 3.1 Growth mechanism

The vapor liquid solid (VLS) technique has been proposed to explain the formation of SnO<sub>2</sub> nanowires. It is well known that the growth of a crystal is always initiated from the nucleation process. For heterogeneous processes, as in the present work, gold particles act as a nucleation sites for the subsequent growth of SnO<sub>2</sub> crystals. The main driving force for the nucleation and growth of crystal is the value of supersaturation of the growth species. In 1D growth processes that produce nanowires, catalysts act as a nucleation site and a higher value of supersaturation of incoming species leads to the growth in one dimension only. The vapors of source material carry high Gibb's free energy which gives rise to its diffusion into the catalyst droplet in order to minimize the energy. The liquid alloy droplet supersaturates with the source material vapors resulting in growth of crystalline structures of source material at the liquid–solid interface (L–S interface) on the surface of substrates, consequently, forming one dimensional nanostructure. The growth kinetics of SnO<sub>2</sub> nanowires by VLS method have been explained earlier by Zhang et al. [26].

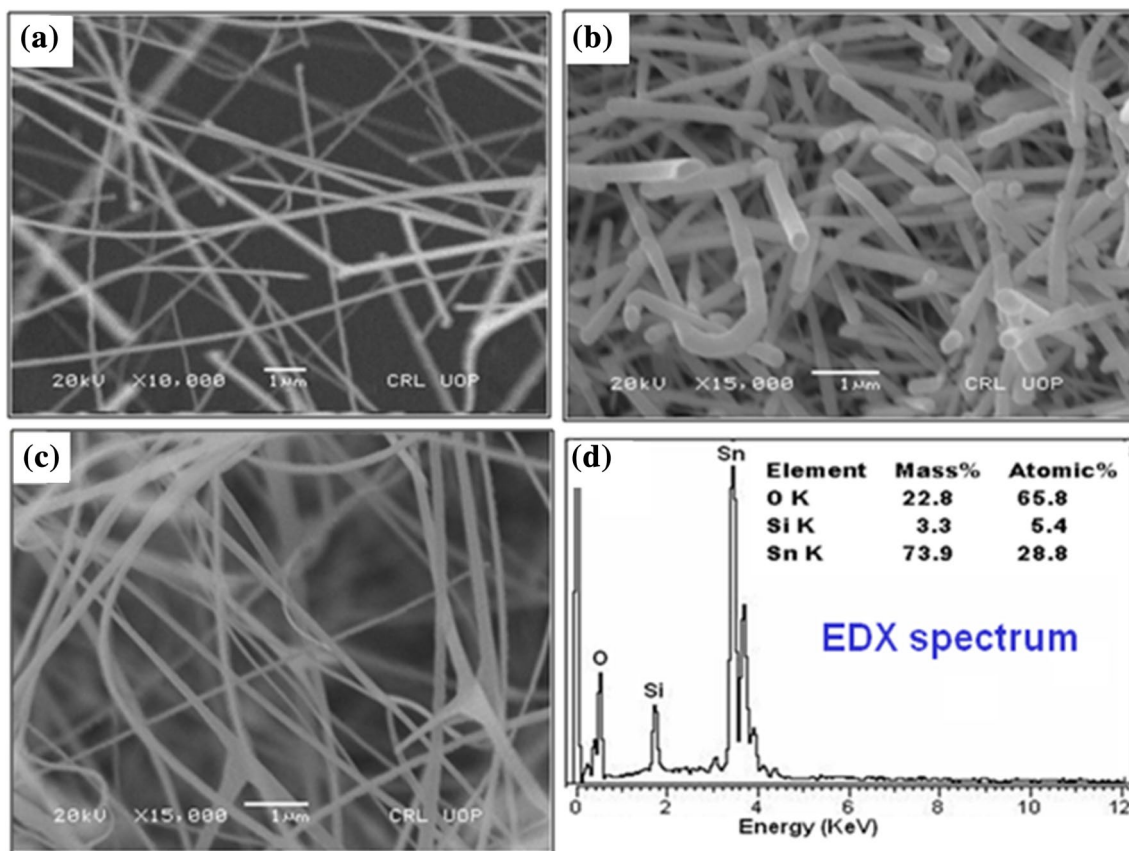
#### 3.2 Morphology and stoichiometry

Figure 2 shows the SEM images of SnO<sub>2</sub> nanowires with three different thicknesses along with EDX spectra

associated with each sample. Figure 2a shows large quantity of the cylindrical nanowires grown on substrate having 1 nm of Au layer are randomly oriented with very high aspect ratio of 384. The average diameter and length of nanowires are  $104 \pm 32$  nm and  $40.3 \pm 14.0$   $\mu$ m, respectively. Figure 2b shows cylindrical nanowires grown on substrate having 2 nm of Au layer are randomly oriented with aspect ratio of 209. The average diameter and length of nanowires are found to be  $127 \pm 30$  nm and  $26.6 \pm 12.3$   $\mu$ m, respectively. The measured aspect ratio for sample three having 5 nm of Au layer is 101. Figure 2c shows nanowires for sample three having average diameter and length of  $198 \pm 19$  nm and  $20.0 \pm 11.8$   $\mu$ m, respectively.

EDX spectrum of SnO<sub>2</sub> nanowires shown in Fig. 2d clearly depicts the tin and oxygen peaks. The approximate atomic ratios are found to be 28:65. The appearance of Si peak is obviously due to the substrate. It can be observed that diameter of the synthesized nanostructures increases with increasing the thickness of catalyst layer. This increment in diameter is due to the availability of larger nucleation sites that increases linearly with thickness of catalyst layer. The presence of nanoparticles on the tips of nanowires is considered to be the evidence of vapor–liquid–solid mechanism [48]. The growth of 1D structure depends on the rate of adsorption of incoming vapors to the catalyst particles, their diffusion and the rate of crystallization at L–S interfaces.

Figure 3a–c show low and high magnification TEM images of SnO<sub>2</sub> nanowires. The TEM image shown in Fig. 3a clearly shows the catalyst particles on the tips of



**Fig. 2** SEM images of SnO<sub>2</sub> Nanowires at 900 °C. **a** Nanowires at 1 nm Au layer. **b** Nanowires at 2 nm Au layer. **c** Nanowires at 5 nm Au layer and **d** EDX spectrum for sample 1

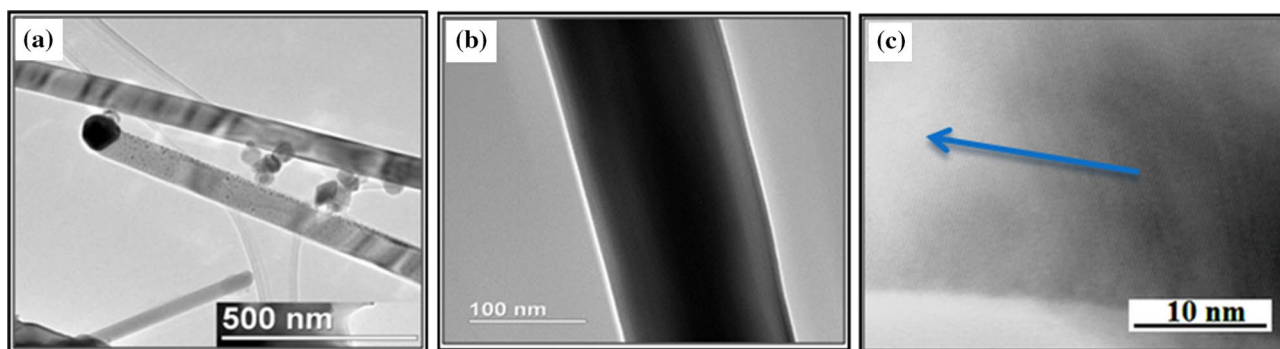


**Fig. 3** TEM images of SnO<sub>2</sub> nanowires for sample 1 (**a**, **b**) at different magnification and (**c**) HRTEM image

the nanowire suggesting the VLS growth. HRTEM image (Fig. 3c) shows the lattice fringes (inter planer spacing = 0.26 nm) of crystalline nanowires suggesting their growth in tetragonal rutile phase of SnO<sub>2</sub>.

### 3.3 XRD analysis

The X-ray diffraction patterns of the synthesized SnO<sub>2</sub> nanowires are shown in Fig. 4. All diffraction peaks

identified correspond to the tetragonal phase of SnO<sub>2</sub>. Measured lattice parameters for three samples are as follows: Sample 1,  $a = b = 4.75 \text{ \AA}$ ,  $c = 3.20 \text{ \AA}$ , Sample 2,  $a = b = 4.74 \text{ \AA}$ ,  $c = 3.20 \text{ \AA}$ , Sample 3,  $a = b = 4.74 \text{ \AA}$ ,  $c = 3.19 \text{ \AA}$ . All calculated parameters are comparable to the standard reported reference data (ICDD 00-041-1445). The sharpness of the XRD patterns reflects the crystallinity of the SnO<sub>2</sub> nanowires. The appearance of diffraction peaks corresponding to Si and SiO<sub>2</sub> is due the substrate's effect. No



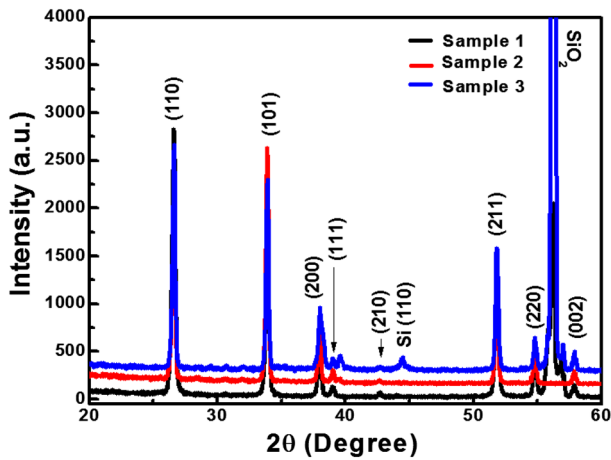


**Fig. 4** XRD patterns of SnO<sub>2</sub> nanowires

diffraction peaks for other impurities are detected in XRD patterns and observed XRD results are consistent with that obtained from TEM.

### 3.4 Optical properties

The optical properties of SnO<sub>2</sub> nanowires have been studied by UV–Vis absorption spectroscopy (lambda 950, UV–Vis spectrophotometer). Figure 5a shows the absorption spectrum for three samples having nanowires of different diameters. The band gap can be calculated by using the Tauc Eq. [49, 50]:

$$\alpha h\nu = A(h\nu - E_g)^{1/2} \tag{1}$$

where A is constant, E<sub>g</sub> is band gap of the nanowires. The band gap was calculated by extrapolating the straight portion of the (αhν)<sup>2</sup> versus hν graph on the photon energy axis at α=0 as shown in Fig. 5c. The inset shows the absorption spectra of nanowires.

The estimated optical energy band gaps of SnO<sub>2</sub> nanowires were found to be 3.76, 3.68 and 3.63 eV for samples with 1, 2 and 5 nm of catalyst thicknesses, respectively. The observed decrement in values band gap with

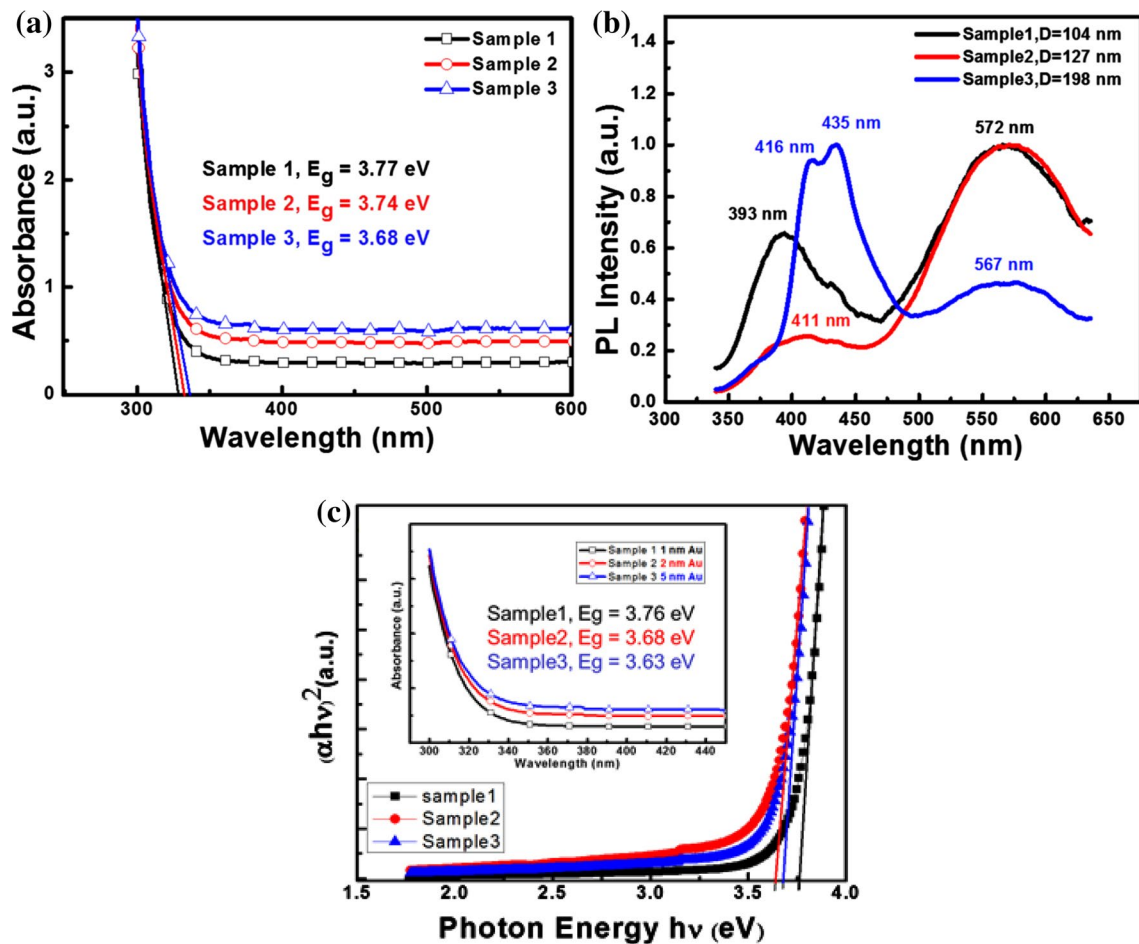


**Fig. 5** a Absorbance spectra. b Room temperature photoluminescence spectra and (c) Band gaps of SnO<sub>2</sub> nanowires

increasing thickness of catalyst layer is in accordance with the observations reported earlier [35, 51].

Figure 5b presents the room temperature photoluminescence (PL) spectra of three samples with He-Cd laser excited at 325 nm. Broad emission peaks at 567 and 572 nm for all three samples suggesting defect-related (O vacancies and Sn interstitials) electronic states within the band gap [52, 53]. Peaks at 393, 411, 416 and 435 nm are due to trapped states within the band gap. Nanowires with smaller diameter (Sample 1) showed a blue shift in emission peak observed at lower wavelength as compared to that observed for samples 2 and 3. This shift is attributed to the production of more defects due to high surface to volume ratio [35]. XRD patterns show a slight shift of diffraction peaks from original values for all three samples. This shift is observed due to the defects like oxygen vacancies and Sn interstitials created during growth process at high temperature. The role of carbon in creation of defects during growth process is also crucial due to carbo-thermal reaction and presence of carrier gas *i.e.* N<sub>2</sub> at high temperature in oxygen deficient environment. Figure 5b represents the PL spectra at room temperature, broad peaks at ~567 and 572 nm are observed in all samples which are believed to originate from the defect-related electronic states in the band gap [46, 53]. In the present work, graphite (carbon) serves both as a catalyst and reducing agent in the reaction. SnO<sub>2</sub> reduces into SnO<sub>x</sub>,  $x < 2$  in the presence of iron. At elevated temperature, it becomes unstable and is converted to SnO and Sn vapors [47]. It is believed in general that SnO is the metastable state and decomposes into Sn and SnO<sub>2</sub> vapors [54]. This decomposition will increase the amount of Sn atoms in the system, whereas SnO<sub>2</sub> deposits onto the silicon substrate providing nucleation sites for the growth [55].

The extent of non-stoichiometry *i.e.* crystal defects in SnO<sub>2</sub> nanowires can be described by intensity ratio of visible luminescence to ultra-violet luminescence ( $I_{vl}/I_{ul}$ ). If  $I_{vl}/I_{ul}$  ratio is higher, there will be more intrinsic defects. The calculated ratio of  $I_{vl}/I_{ul}$  for the present study is 4.0, 1.5 and 0.46 for samples 1, 2 and 3, respectively. The systematic decrement observed in the value of emission intensities reveals that defects are upsurges with increase in diameter of nanowires.

These results are consistent with gas sensing response of SnO<sub>2</sub> nanowires presenting that PL emission and decay time strongly depend on the shape of the nanocrystals [56, 57].

### 3.5 Gas sensing mechanism

The sensing mechanism is based on the principal of change in electrical resistivity/conductivity as a result of chemical reaction between gas molecules and the reactive oxygen ions on the surface of SnO<sub>2</sub> nanowires. When air is flown over the surface of SnO<sub>2</sub> nanowires the oxygen ions are attached at the surface by capturing electrons from conduction band [58, 59]. At high temperature, reactive oxygen species (O<sup>2-</sup>, O<sub>2</sub><sup>-</sup> and O<sup>-</sup>) are chemisorbed by these nanowires resulted in electron transfer. At a certain level of adsorption, a thick depletion layer is formed on the surface due to which resistance of the material is increased. In contrast, when SnO<sub>2</sub> nanowires are exposed to the CO gas, adsorbed oxygen ions produce CO<sub>2</sub> which ultimately reduces the resistance and enhances the carriers concentration [60].

As metal oxide nanostructures are known to differ much in their stoichiometry due to their rich defects chemistry which means that, although they may have been grown through the same process, the three samples of the nanowires can have different charge carrier densities which lead to different  $L_d$  values according to relation in Eq. (2).

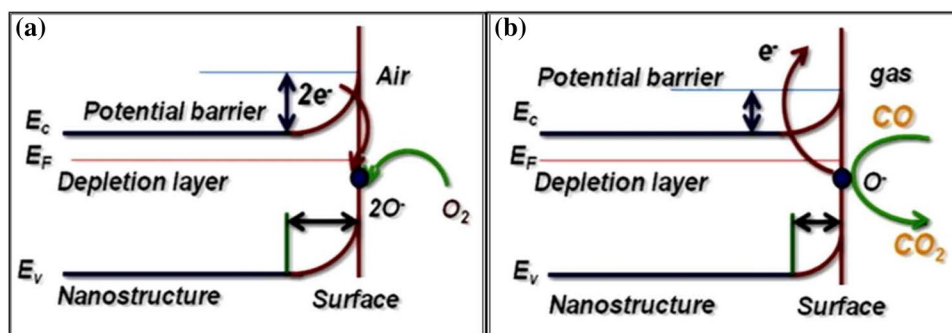
$$L_d = (\epsilon\epsilon_0 kT / e^2 n_0)^{1/2} \quad (2)$$

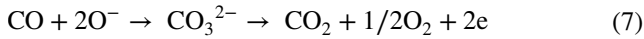
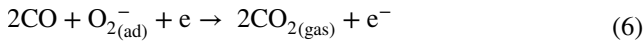
The Debye length of the material is generally used to give an estimate for the width of space-charge layer for metal-oxides used in gas sensor technology [61].

The mechanism is schematically presented in Fig. 6 and can be summarized by the following chemical reactions:



**Fig. 6** Schematic of possible mechanism of SnO<sub>2</sub> nanowires sensor responses to CO in air (a) and gas (b)





### 3.6 Gas sensing properties

Figure 7a–c shows the sensing response signals of SnO<sub>2</sub> nanowires for CO gas, CH<sub>4</sub> gas and Methanol respectively as a function of catalyst thickness for three samples. The sensing experiments were performed at 300 °C with 3 min cycles of dry air for 20 ppm CO gas and interference gases (400 ppm CH<sub>4</sub> gas and 200 ppm Methanol) for comparison [62, 63]. Figure 7a shows decrement in resistance upon exposure to CO and recovered completely to the initial value upon removal of CO. Sensing response of the nanowires is found to be 3.35, 2.58 and 2.32 for aspect ratios 384, 209 and 101, respectively. Sensing response to CH<sub>4</sub> gas is 1.20, 1.09 and 1.05, respectively

for above mentioned aspect ratios (Fig. 7b). For methanol gas observed sensing response is 2.61, 2.33 and 1.80 for three aspect ratios, respectively (Fig. 7c). Selectivity of SnO<sub>2</sub> nanowires is shown in Fig. 7d.

Summary of the gas sensing results are shown in Table 1 and Colum graph in Fig. 7e. Gas sensing results demonstrate that sensing response increases with increase in aspect ratio and decrease in diameter of the nanowires. Gas sensor shows sensitive and a little bit selective response to CO gas compared to other test gases. The high response of SnO<sub>2</sub> nanowires for three gases is due to high surface to volume ratio, which could provide more active sites at the surface for oxygen adsorption or to contact with surrounding gases [64, 65]. Presented results illustrate an improved sensing response compared to that reported earlier with respect to gas sensing response and limit of detection as shown in Table 2.

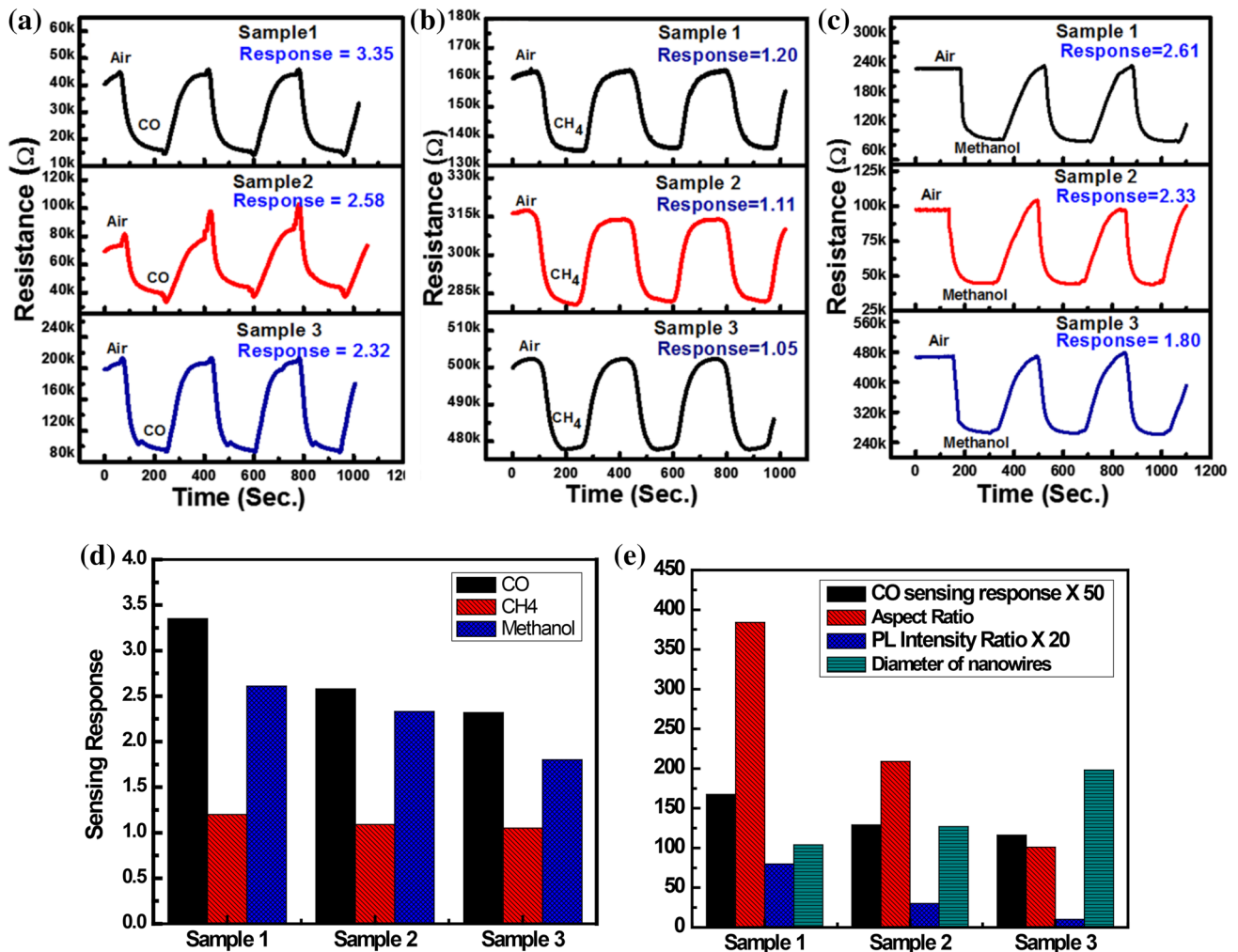


**Fig. 7** Time dependent gas sensing responses of SnO<sub>2</sub> Nanowires at 300 °C for three samples, a 20 ppm of CO gas (b) 400 ppm of CH<sub>4</sub> gas, c 200 ppm of Methanol and d Selectivity of SnO<sub>2</sub> nanowires. e Comparison graph of all results of SnO<sub>2</sub> nanowires

**Table 1** Summary of gas sensing results

Sample no.	Gas sensing response ( $S = R_a/R_g$ )			Properties		
	CO (20 ppm, 300 °C)	CH <sub>4</sub> (400 ppm, 300 °C)	Methanol (200 ppm, 300 °C)	Aspect ratio (L/D)	PL intensity ratio ( $I_{vl}/I_{ul}$ )	Diameter (nm)
1	3.35	1.20	2.61	384	4.0	104 ± 32
2	2.58	1.09	2.33	209	1.5	127 ± 30
3	2.32	1.05	1.80	101	0.5	198 ± 19

**Table 2** Comparison with reported SnO<sub>2</sub> nanowires CO gas sensors

Sensor description	CO concentration	Gas response	T (°C)	References
Network SnO <sub>2</sub> NWs (CVD)	20 ppm	$R_a/R_g \sim 3.35$	300	Present work
Single SnO <sub>2</sub> NWs (CVD)	100 ppm	$R_a/R_g \sim 2.0$	250–400	[33]
	100 ppm	$G_a/G_g \sim 1.9$		[34]
	500 ppm	$R_a/R_g \sim 1.2$		[35]
Screen printed SnO <sub>2</sub> NWs (CVD)	100 ppm	$R_a/R_g \sim 2.9$	400	[36]
Network SnO <sub>2</sub> NWs	100 ppm	$R_a/R_g \sim 1.8$	350	[29]
Network SnO <sub>2</sub> NWs	100 ppm	$R_a/R_g \sim 1.32$	380	[37]
SnO <sub>2</sub> NWs (CVD)	400 ppm	$R_a/R_g \sim 3.9$	400	[38]

## 4 Conclusions

Size controlled SnO<sub>2</sub> nanowires (NWs) have been synthesized by a simple vapor transport method by modulating the thickness of Au layer as catalyst. XRD peaks indicated the crystalline quality of nanowires. SEM images revealed that the nanowires are in cylindrical form with high aspect ratio. TEM and HRTEM images confirmed the VLS growth of SnO<sub>2</sub> nanowires consistent to XRD results. The photoluminescence and optical properties provided the bandgap energies and surface defects of deposited nanowires. The gas sensing results revealed a sensitive and selective response of nanowires sensors to 20 ppm of CO gas at 300 °C compared to other test gases. Maximum value of sensing response was found to be 3.35 for the nanowires with aspect ratio of 384. This improved sensing response is attributed to the large number of active sites for oxygen adsorption resulted from high aspect ratio and large surface to volume ratio of SnO<sub>2</sub> nanowires. These sensors have potential applications in modern and advanced gas sensing devices.

**Acknowledgements** Authors would like to acknowledge Higher Education Commission (HEC) of Pakistan for providing financial support through “National Research Program for Universities” and CIIT, Islamabad for providing funds under project # 16-27/CRGP/CIIT/IBD/13/225. One of the authors (Muhammad Amin) acknowledges the HEC of Pakistan for the award of Indigenous PhD scholarship in batch-IV and IRSIP.

## References

1. S. Iijima, Helical microtubules of graphitic carbon. *nature* **354**(6348), 56–58 (1991)
2. B. Tian, T.J. Kempa, C.M. Lieber, Single nanowire photovoltaics. *Chem. Soc. Rev.* **38**(1), 16–24 (2009)
3. C.M. Lieber, Z.L. Wang, Functional nanowires. *MRS Bull.* **32**(02), 99–108 (2007)
4. G. Korotcenkov, Metal oxides for solid-state gas sensors: What determines our choice? *Mater. Sci. Eng. B* **139**(1), 1–23 (2007)
5. V. Malyshev, A. Pislyakov, Investigation of gas-sensitivity of sensor structures to carbon monoxide in a wide range of temperature, concentration and humidity of gas medium. *Sens. Actuators B* **123**(1), 71–81 (2007)
6. Q.-H. Wu, J. Li, S.-G. Sun, Nano SnO<sub>2</sub> gas sensors. *Curr. Nanosci.* **6**(5), 525–538 (2010)
7. M.E. Franke, T.J. Koplín, U. Simon, Metal and metal oxide nanoparticles in chemiresistors: does the nanoscale matter? *Small* **2**(1), 36–50 (2006)
8. C. Xu et al., Grain size effects on gas sensitivity of porous SnO<sub>2</sub>-based elements. *Sens. Actuators B* **3**(2), 147–155 (1991)
9. K. Soulantica et al., Synthesis of indium and indium oxide nanoparticles from indium cyclopentadienyl precursor and their application for gas sensing. *Adv. Funct. Mater.* **13**(7), 553–557 (2003)
10. Y.-J. Choi et al., Novel fabrication of an SnO<sub>2</sub> nanowire gas sensor with high sensitivity. *Nanotechnology* **19**(9), 095508 (2008)
11. I.-D. Kim et al., Ultrasensitive chemiresistors based on electrospun TiO<sub>2</sub> nanofibers. *Nano Lett.* **6**(9), 2009–2013 (2006)
12. M. Tonezzer, N. Hieu, Size-dependent response of single-nanowire gas sensors. *Sens. Actuators B* **163**(1), 146–152 (2012)
13. A. Vomiero et al., Controlled growth and sensing properties of In<sub>2</sub>O<sub>3</sub> nanowires. *Cryst. Growth Des.* **7**(12), 2500–2504 (2007)



14. W.-Y. Li, L.-N. Xu, J. Chen,  $\text{Co}_3\text{O}_4$  nanomaterials in lithium-ion batteries and gas sensors. *Adv. Funct. Mater.* **15**(5), 851–857 (2005)
15. R. Afrin et al., Design and analysis of functional multiwalled carbon nanotubes for infrared sensors. *Sens. Actuators A* **203**, 142–148 (2013)
16. J. Zhang et al., Microwave-assisted and large-scale synthesis of  $\text{SnO}_2$ /carbon-nanotube hybrids with high lithium storage capacity. *RSC Adv.* **5**(72), 58568–58573 (2015)
17. E. Comini et al., Stable and highly sensitive gas sensors based on semiconducting oxide nanobelts. *Appl. Phys. Lett.* **81**, 1869–1871 (2002)
18. S. Zia et al., Ultra-long multicolor belts and unique morphologies of tin-doped zinc oxide nanostructures. *Appl. Phys. A* **115**(1), 275–281 (2014)
19. F.K. Butt et al., Metal-catalyzed synthesis of ultralong tin dioxide nanobelts: electrical and optical properties with oxygen vacancy-related orange emission. *Mater. Sci. Semicond. Process.* **26**, 388–394 (2014)
20. M. Amin et al., Effects of Mg doping on optical and CO gas sensing properties of sensitive ZnO nanobelts. *CrystEngComm* **16**(27), 6080–6088 (2014)
21. N. Yamazoe, New approaches for improving semiconductor gas sensors. *Sens. Actuators B* **5**(1–4), 7–19 (1991)
22. Y.-F. Sun et al., Metal oxide nanostructures and their gas sensing properties: a review. *Sensors* **12**(3), 2610–2631 (2012)
23. S.M. Sedghi, Y. Mortazavi, A. Khodadadi, Low temperature CO and  $\text{CH}_4$  dual selective gas sensor using  $\text{SnO}_2$  quantum dots prepared by sonochemical method. *Sens. Actuators B* **145**(1), 7–12 (2010)
24. N. Yamazoe, G. Sakai, K. Shimano, Oxide semiconductor gas sensors. *Catal. Surv. Asia* **7**(1), 63–75 (2003)
25. F. Hernandez-Ramirez et al., High response and stability in CO and humidity measures using a single  $\text{SnO}_2$  nanowire. *Sens. Actuators B* **121**(1), 3–17 (2007)
26. D.-F. Zhang et al., Size-controllable one-dimensional  $\text{SnO}_2$  nanocrystals: synthesis, growth mechanism, and gas sensing property. *Phys. Chem. Chem. Phys.* **8**(42), 4874–4880 (2006)
27. Q. Lipeng et al., The template-free synthesis of square-shaped  $\text{SnO}_2$  nanowires: the temperature effect and acetone gas sensors. *Nanotechnology* **19**(18), 185705 (2008)
28. A. Kolmakov et al., Enhanced Gas sensing by individual  $\text{SnO}_2$  nanowires and nanobelts functionalized with Pd catalyst particles. *Nano Lett.* **5**(4), 667–673 (2005)
29. Y.J. Kwon et al., Selective improvement of  $\text{NO}_2$  gas sensing behavior in  $\text{SnO}_2$  nanowires by ion-beam irradiation. *ACS Appl. Mater. Interfaces* **8**(21), 13646–13658 (2016)
30. J. Wu et al., Controllable synthesis and field emission properties of  $\text{SnO}_2$  zigzag nanobelts. *J. Phys. D: Appl. Phys.* **41**(18), 185302 (2008)
31. T. Van Dang et al., Chlorine gas sensing performance of on-chip grown ZnO,  $\text{WO}_3$ , and  $\text{SnO}_2$  nanowire sensors. *ACS Appl. Mater. Interfaces* **8**(7), 4828–4837 (2016)
32. J. Zheng et al., Modeling and Simulation of Single Nanobelt  $\text{SnO}_2$  Gas Sensors with FET Structure. *Sens. Actuators B* **128**, 226–234 (2007)
33. Z.P. Guo et al., Ultra-fine porous  $\text{SnO}_2$  nanopowder prepared via a molten salt process: a highly efficient anode material for lithium-ion batteries. *J. Mater. Chem.* **19**(20), 3253–3257 (2009)
34. N. Bhardwaj, S. Kuriakose, S. Mohapatra, Structural and optical properties of  $\text{SnO}_2$  nanotowers and interconnected nanowires prepared by carbothermal reduction method. *J. Alloys Compd.* **592**, 238–243 (2014)
35. S. Luo et al., Synthesis and low-temperature photoluminescence properties of  $\text{SnO}_2$  nanowires and nanobelts. *Nanotechnology* **17**(6), 1695 (2006)
36. Y. Chen et al., Bulk-quantity synthesis and self-catalytic VLS growth of  $\text{SnO}_2$  nanowires by lower-temperature evaporation. *Chem. Phys. Lett.* **369**(1), 16–20 (2003)
37. Y. Chen, L. Campbell, W. Zhou, Self-catalytic branch growth of  $\text{SnO}_2$  nanowire junctions. *J. Cryst. Growth* **270**(3), 505–510 (2004)
38. C. Ling, W. Qian, F. Wei, Gas-flow assisted bulk synthesis of V-type  $\text{SnO}_2$  nanowires. *J. Cryst. Growth* **285**(1), 49–53 (2005)
39. D. Calestani et al., Structural and optical study of  $\text{SnO}_2$  nanobelts and nanowires. *Mater. Sci. Eng. C* **25**(5), 625–630 (2005)
40. M.O. Orlandi et al., Growth of  $\text{SnO}$  nanobelts and dendrites by a self-catalytic VLS process. *J. Phys. Chem. B* **110**(13), 6621–6625 (2006)
41. R. Yang, Z.L. Wang, Springs, rings, and spirals of rutile-structured tin oxide nanobelts. *J. Am. Chem. Soc.* **128**(5), 1466–1467 (2006)
42. P. Nguyen, H.T. Ng, M. Meyyappan, Catalyst metal selection for synthesis of inorganic nanowires. *Adv. Mater.* **17**(14), 1773–1777 (2005)
43. J. Wang et al., Growth of  $\text{SnO}_2$  nanowires with uniform branched structures. *Solid State Commun.* **130**(1), 89–94 (2004)
44. B. Wang et al., Nanostructures and self-catalyzed growth of  $\text{SnO}_2$ . *J. Appl. Phys.* **98**(7), 073520 (2005)
45. S. Budak et al., Growth and characterization of single crystalline tin oxide ( $\text{SnO}$ ) nanowires. *J. Cryst. Growth* **291**(2), 405–411 (2006)
46. Z. Zhang et al., Morphology-controlled synthesis and a comparative study of the physical properties of  $\text{SnO}_2$  nanostructures: from ultrathin nanowires to ultrawide nanobelts. *Nanotechnology* **20**(13), 135605 (2009)
47. F.K. Butt et al., Fabrication of novel  $\text{SnO}_2$  nanofibers bundle and their optical properties. *Mater. Chem. Phys.* **136**(1), 10–14 (2012)
48. F. Yu et al., Fabrication of  $\text{SnO}_2$  one-dimensional nanostructures with graded diameters by chemical vapor deposition method. *J. Cryst. Growth* **312**(2), 220–225 (2010)
49. F.K. Butt et al., Synthesis of highly pure single crystalline  $\text{SnSe}$  nanostructures by thermal evaporation and condensation route. *Mater. Chem. Phys.* **137**(2), 565–570 (2012)
50. W.S. Khan et al., Optical properties and characterization of zinc nitride nanoneedles prepared from ball-milled Zn powders. *Mater. Lett.* **65**(9), 1264–1267 (2011)
51. S. Mathur et al., Size-dependent photoconductance in  $\text{SnO}_2$  nanowires. *Small* **1**(7), 713–717 (2005)
52. S. Luo et al., Origin of low-temperature photoluminescence from  $\text{SnO}_2$  nanowires fabricated by thermal evaporation and annealed in different ambients. *Appl. Phys. Lett.* **88**(18), 3112 (2006)
53. H. He Jr. et al., Beaklike  $\text{SnO}_2$  nanorods with strong photoluminescent and field-emission properties. *Small* **2**(1), 116–120 (2006)
54. J. Hu et al., Large-scale rapid oxidation synthesis of  $\text{SnO}_2$  nanoribbons. *J. Phys. Chem. B* **106**(15), 3823–3826 (2002)
55. F.K. Butt et al., Electrical and optical properties of single zigzag  $\text{SnO}_2$  nanobelts. *CrystEngComm* **15**(11), 2106–2112 (2013)
56. J. Hu et al., Laser-ablation growth and optical properties of wide and long single-crystal  $\text{SnO}_2$  Ribbons. *Adv. Funct. Mater.* **13**(6), 493–496 (2003)
57. A. Kar, S. Kundu, A. Patra, Surface defect-related luminescence properties of  $\text{SnO}_2$  nanorods and nanoparticles. *J. Phys. Chem. C* **115**(1), 118–124 (2010)
58. G. Dar et al., Ce-doped ZnO nanorods for the detection of hazardous chemical. *Sens. Actuators B* **173**, 72–78 (2012)
59. N. Han et al., Evaluating the doping effect of Fe, Ti and Sn on gas sensing property of ZnO. *Sens. Actuators B* **147**(2), 525–530 (2010)
60. J. Li, H. Fan, X. Jia, Multilayered ZnO nanosheets with 3D porous architectures: synthesis and gas sensing application. *J. Phys. Chem. C* **114**(35), 14684–14691 (2010)

61. D.E. Williams, K.F. Pratt, Microstructure effects on the response of gas-sensitive resistors based on semiconducting oxides. *Sens. Actuators B* **70**(1), 214–221 (2000)
62. H.S. Hong et al., Selective detection of carbon dioxide using LaOCl-functionalized SnO<sub>2</sub> nanowires for air-quality monitoring. *Talanta* **88**, 152–159 (2012)
63. B. Bahrami et al., Enhanced CO sensitivity and selectivity of gold nanoparticles-doped SnO<sub>2</sub> sensor in presence of propane and methane. *Sens. Actuators B* **133**(1), 352–356 (2008)
64. B. Shouli et al., Different morphologies of ZnO nanorods and their sensing property. *Sens. Actuators, B* **146**(1), 129–137 (2010)
65. Y. Shen et al., Influence of effective surface area on gas sensing properties of WO<sub>3</sub> sputtered thin films. *Thin Solid Films* **517**(6), 2069–2072 (2009)